Journal of Materials Chemistry

View Online
Dynamic Article Links

Cite this: J. Mater. Chem., 2011, 21, 4235

www.rsc.org/materials

PAPER

Size-controlled synthesis of $BiPO_4$ nanocrystals for enhanced photocatalytic performance†

Chengsi Pan and Yongfa Zhu*

Received 27th October 2010, Accepted 21st December 2010
DOI: 10.1039/c0jm03655b

Well dispersed $BiPO_4$ nanocrystals with a diameter of ~9 nm are synthesized in oleic acid (OA) and bis(2-ethylhexyl) phosphate (BEHP) media by a high-temperature hydrolysis reaction. OA absorbed on the surface of the nanocrystals helps make a monodispersion. In this reaction, the diameters of the as prepared $BiPO_4$ nanocrystals can be controlled from 9 nm to 250 nm by changing the OA/BEHP ratio (v/v). The roles of BEHP and OA during the formation of the nanocrystals and for tuning the grain size of the particles have been discussed, and a possible formation mechanism of the nanocrystals is proposed. $BiPO_4$ nanocrystals with a diameter of ~9 nm after OA removal show the highest activity for degradation of methylene blue solution in the UV region, which is also nearly twice the reported activity of $BiPO_4$, and 2.6 times higher than that of P25. The high Brunauer–Emmett–Teller (BET) surface, large band gap, surface effect, and short mobility distance for carriers to the surface are recognized as the key factors for the high photocatalytic activity of nanocrystals.

1. Introduction

Since the 1990s much attention has been paid to colloidal semiconductor nanocrystals due to their promising optical applications in photonics,[1] photovoltaics,[2,3] light-emitting diodes,[4] and photoluminescence devices.[5–7] For semiconductor photocatalysis, they are even more attractive, such as the most applied nanocrystal photocatalytic material, P25 (TiO_2). They are widely used in photocatalysis due to their unique size-dependent optical and electrical properties. Compared to the bulk materials, nanocrystals exhibiting properties such as band gap broadening,[8] large surface/volume ratio,[9] as well as short mobility distance for carriers to the nanocrystal surface,[10] are considered as beneficial for the separation and transfer of photogenerated e^-/h^+.[11] Therefore, except for P25, nanocrystals of other photocatalysts are synthesized with the aim that they will achieve maximum photocatalytic activity, because the photocatalytic activity of P25 is not high enough to meet industrial use.

In spite of extensive research on such new photocatalytic systems in the past, only a few of them exhibit high photocatalytic activity (compared to the commercial TiO_2, P25). In the past ten years, Bi-based photocatalysts have been shown to exhibit a superior photocatalytic activity than P25 in both the UV and VIS regions. This activity is closely related to their size and morphology. For example, Bi_2WO_6 and $BiVO_4$ nanosheets, reported by us and other groups show a much higher photocatalytic activity than the bulk ones.[12–20] This kind of ultrathin nanosheet is just several nanometres thick, which is beneficial for the separation and transfer of the photogenerated e^-/h^+ as reported in the $Ba_5Ta_4O_{15}$ system.[21] Also in the Bi_2WO_6 system, small-sized Bi_2WO_6 nanosheets (~20 nm) perform better in photocatalytic activity than the larger ones (~1 μm) due to a higher BET surface.[22] However, it must be point out that due to the lamellar structure of most of Bi salts, the size control of Bi salts is often in one dimension (*e.g.* ultrathin nanosheets) not in zero dimension (*e.g.* nanocrystals). Furthermore, much work needs to be done in terms of improving overall control in size distribution of Bi salt nanocrystals, especially for the synthesis of small-sized nanocrystals ($D < 10$ nm). Within that size, nanosize effects can be considered as the main factors that influence the photocatalytic activity. Only a few papers, rarely related to photocatalysis, have reported the successful preparation of Bi salt nanocrystals, mostly sulfide or telluride, such as $NaPb_{13}Sn_5BiTe_{20}$,[23] $AgBiS_2$.[24] In fact, the major issue in preparing Bi-based salt nanocrystals is the lack of salt precursors to match the very active Bi-based precursor, because the Bi^{3+} cation has a strong tendency toward hydrolysis. As a result, to avoid hydrolysis, the synthesis of monodispersed Bi salt nanocrystal needs expensive Bi metal–organic salts or specific synthesis methods, such as the sonochemical method.[24] Therefore, the development of an ordinary method for size-controlled synthesis of Bi salt nanocrystals from cheap source materials presents a great challenge.

One of the Bi salts, $BiPO_4$, synthesized by hydrothermal reaction ($BiPO_4$-HT), has a good photocatalytic performance which is as much as twice that of P25, as recently reported by our

Department of Chemistry, Tsinghua University, Beijing, 100084, P.R. China. E-mail: zhuyf@mail.tsinghua.edu.cn; Fax: +86-10-62787601; Tel: +86-10-62783586

† Electronic supplementary information (ESI) available: Detailed experimental procedures, and additional figures. See DOI: 10.1039/c0jm03655b

group.[25] However, its Brunauer–Emmett–Teller (BET) surface area (3 $m^2 g^{-1}$) is just one sixteenth of P25 (50 $m^2 g^{-1}$) due to the large diameter of the former (~100 nm). In other previous papers, $BiPO_4$ synthesized by electrochemical deposition,[26] CVD,[27] mechanical ball milling,[28] high-temperature solid reaction[29] all showed a large size, more than 50 nm. Recently, Roming and Feldmann reported the formation of $BiPO_4$ nanocrystals with a size of 37 nm using polyol-mediated synthesis.[30] However, there are still no reports on synthesis of well dispersed $BiPO_4$ nanocrystals (D < 10 nm).

In this paper, well dispersed $BiPO_4$ nanocrystals with a size of ~9 nm are synthesized in oleic acid (OA) and bis(2-ethylhexyl) phosphate (BEHP) media by a high-temperature hydrolysis reaction. In this reaction, the diameters of the as prepared $BiPO_4$ nanocrystals can be controlled ranging from 9 nm to 200 nm as the OA/BEHP ratio (v/v) changes. The calcined $BiPO_4$ nanocrystals (~9 nm) showed the highest activity for degradation of methylene blue (MB) solution of all the prepared $BiPO_4$ nanocrystals, which was also higher than that of the $BiPO_4$-HT and P25 we reported before.[25] The small size of $BiPO_4$ nanocrystals are recognized as the key factor for the high photocatalytic activity. Additionally, the synthesis of phosphate salt nanocrystals often utilises an inorganic phosphoric source,[31,32] which is hard to dissolve in the organic solvents in which most nanocrystals are prepared. This leads to complex steps or systems for the formation and control of phosphate salt nanocrystals. The use of a phosphate ester in this paper, which is easily soluble in organic solvents, demonstrates a new kind of phosphate source potentially applicable to the synthesis of other phosphate salt nanocrystals.

2. Experimental section

2.1 Synthesis

$BiPO_4$ nanocrystal synthesis. The synthesis was carried out using standard oxygen-free procedures. All chemicals used were analytic grade reagents without further purification. For a typical preparation, $Bi(NO_3)_3 \cdot 5H_2O$ (0.5 mmol) was added into a 40 ml mixed solvent of oleic acid (OA) and bis(2-ethylhexyl) phosphate ($((CH_3(CH_2)_3CH(C_2H_5)CH_2O)_2P(O)OH$, BEHP) with a volume ratio of 38/2 in a three-necked flask at room temperature and then magnetically stirred for 24 h to form a transparent solution at room temperature. The stock solution was bubbled in a N_2 atmosphere for 20 min and then vacuumed at *ca.* 80 °C for 30 min to remove adsorbed water. The flask was then heated to 190 °C at a rate of 20 °C min^{-1} and maintained at this temperature for 2 h under a N_2 atmosphere. When the reaction completed, an excess amount (~40 ml) of ethanol was poured into the solution at *ca.* 70 °C. This solution was separated by centrifugation, and the products were collected. The as-precipitated nanocrystals were washed with ethanol several times and then dried in air at 70 °C overnight. The yield of the as-dried nanocrystals was more than 70%. The as-precipitated nanocrystals could be redispersed in non-polar solvents (*e.g.*, cyclohexane).

OA removal on $BiPO_4$ nanocrystals' surface. The above prepared $BiPO_4$ nanocrystals were loaded in alumina boats in a tube furnace and were annealed at 450 °C for 3 h under atmospheric pressure O_2 to yield $BiPO_4$ nanocrystals without OA.

$BiPO_4$ hydrothermal synthesis ($BiPO_4$-HT). $BiPO_4$ was synthesized through a hydrothermal process according to ref. 25 as a SSR sample. $Bi(NO_3)_3 \cdot 5H_2O$ and equal molar $Na_3PO_4 \cdot 12H_2O$ were put into a beaker. Then, 30 mL of distilled water was added to the beaker and magnetically stirred to form a homogeneous solution at room temperature. The pH was adjusted to 1 by the addition of concentrated HNO_3. The resulting precursor suspension was transferred into a Teflon-lined stainless steel autoclave. The autoclave was sealed and maintained at 180 °C for 72 h, then allowed to cool naturally to room temperature. The products were washed several times with distilled water, and dried at for 24 h, subsequently. The as-prepared sample was 400 ± 100 nm in length and 80 ± 20 nm in diameter.[25]

2.2 Characterization

The products were characterized by powder X-ray diffraction (XRD) on a Bruker D8-advance X-ray diffractometer at 40 kV and 40 mA for monochromatized Cu K_α1 (λ = 1.5406 Å) radiation. Fourier transformed infrared (FT-IR) spectra were recorded on a Thermo Nicolet Avatar 370 spectrometer between 4000 and 450 cm^{-1} using KBr pellets. Morphologies and structures of the prepared samples were further examined with transmission electron microscopy (TEM) by a JEM 1010 electron microscope operated at an accelerating voltage of 100 kV. High-resolution TEM (HRTEM) images were obtained with a JEM 2010F field emission gun transmission electron microscope operated at an accelerating voltage of 200 kV. UV–vis diffuse reflectance spectra (DRS) of the samples were measured by using an Hitachi U-3010 UV–vis spectrophotometer. The Brunauer–Emmett–Teller (BET) specific surface area of the samples was characterized by nitrogen adsorption at 77 K with Micromeritics 3020.

2.3 Photocatalytic evaluation

Photocatalytic activities of $BiPO_4$ were evaluated by degradation of methylene blue (MB) under ultraviolet light irradiation using an 11 W low-pressure lamp at 254 nm. The average light intensity was 1.5 mW cm^{-2}. The radiant flux was measured with a power meter from Institute of Electric Light Source (Beijing). MB solutions (200 ml, 10^{-5} mol L^{-1}) containing 0.100 g of $BiPO_4$ were put in a glass beaker. Before the light was turned on, the solution was first ultrasonicated for 10 min, and then stirred for 10 min to reach absorption–desorption equilibrium (Fig. S1, ESI†). Three millilitres of sample solution were taken at given time intervals and separated through centrifugation (4000 rpm, 10 min). The supernatants were analyzed by recording variations of the absorption band maximum (664 nm) in the UV–vis spectra of MB using a U-3010 spectrophotometer (Hitachi).

3 Results and discussion

3.1 Formation of $BiPO_4$ nanocrystals

Well dispersed $BiPO_4$ nanocrystals can be synthesized by a one-step high-temperature hydrolysis method. Fig. 1 shows the TEM and HRTEM images of the $BiPO_4$ nanocrystals before and after calcination. All the images show that the $BiPO_4$ nanocrystals have a uniform structure with a diameter of ~9 nm. Fig. 1a and 1b show before calcination most of the $BiPO_4$ nanocrystals were well dispersed, and the nanocrystals can form a stable sol even after three month (Fig. S2, ESI†), due to OA absorbed on the surface of the nanocrystals. Unfortunately, the OA will act as a hole scavenger, which decreases the photocatalytic activity. Therefore, the OA must be removed from the surface of nanocrystals by calcination (Fig. 1c and 1d). After OA removal, the $BiPO_4$ nanocrystals are easily aggregated but with almost the same size. The OA removal can also be demonstrated by IR spectra (Fig. S3, ESI†), which shows no peaks owned by CH_2, CH_3, and COO^- at 2850, 2950, and 1640 cm^{-1} after calcination. It is also noted that there are no peaks between 1200 cm^{-1} and 1300 cm^{-1}, which can be attributed to the C–O–P stretch vibration in BEHP. This implies that there is almost no BEHP absorbed on the surface of the nanocrystals. HRTEM images (Fig. 1b and 1d) show that most of the $BiPO_4$ nanocrystals display a cross-lattice pattern with a lattice spacing of 0.416 nm, corresponding to the interplanar separation between the {−111} lattice planes of monoclinic $BiPO_4$.

Fig. 2 shows the XRD pattern of $BiPO_4$ nanocrystals. The sample exhibits feature peaks that correspond to the planes of a monoclinic $BiPO_4$ structure (space group: P21/n) as identified using the standard data JCPDS 80-0209. The value of the lattice parameter calculated from the XRD spectra is $a = 0.6742$ nm, $b = 0.6905$ nm, $c = 0.6470$ nm which is lower than that reported for the bulk $BiPO_4$ in the standard card ($a = 0.6763$ nm, $b = 0.6952$ nm, $c = 0.6482$ nm). The OA groups may stabilize the small nanoparticles resulting in the smaller value of the lattice parameters in our sample, similar to the results reported by Maensiri *et al.*[33] The crystal size of the $BiPO_4$ nanocrystals is about 8.7 nm which is almost near to the size of the nanocrystals observed from the TEM. After OA removal the crystal size of nanocrystals is almost the same, but the peak intensity is obviously higher, which implies a better crystalline form under calcination.

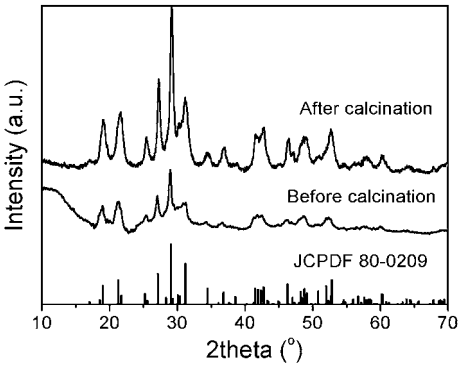

Fig. 2 XRD patterns of $BiPO_4$ nanocrystals before and after OA removal.

Fig. 3 shows typical diffuse reflection spectra (DRS) of good-quality $BiPO_4$ nanocrystals ($BiPO_4$ nc) before and after calcination compared to the hydrothermal reaction sample ($BiPO_4$-HT). The absorption of $BiPO_4$ nanocrystals ranging widely from 400 nm to 200 nm suggests that more absorption states or defect energy bands exist in the well dispersed $BiPO_4$ nanocrystals.[34] Whereas, after calcination the steep shape of the spectra of $BiPO_4$ nanocrystals indicates that the light absorption is not due to the transition from the impurity level but due to the band-gap transition. This is consistent with the XRD results. Compared to the $BiPO_4$-HT sample, the absorption of calcined $BiPO_4$ nanocrystals appears to blue shift obviously. The band gap of the nanocrystals is estimated to be 4.60 eV from the onset of the absorption edge,[35] which was much bigger than that of the $BiPO_4$-HT sample (3.85 eV). This can be attributed to the nanosize effect. The calcined $BiPO_4$ nanocrystals show an intense band centered at ~255 nm and ~230 nm. The former peak can be

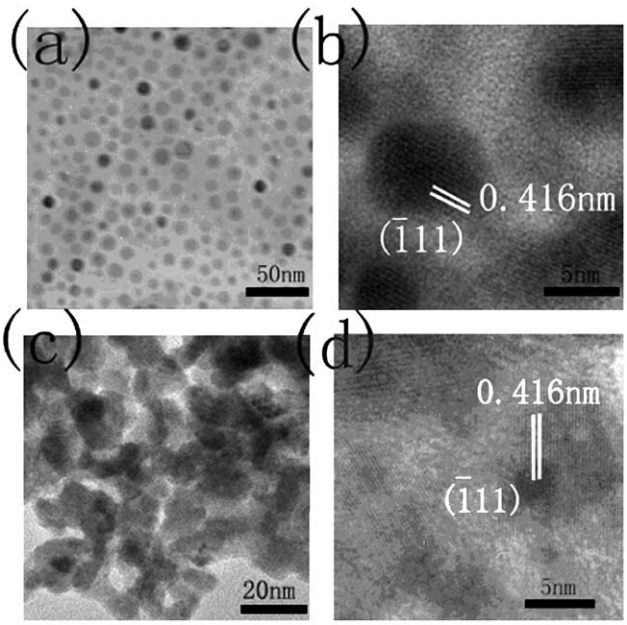

Fig. 1 TEM and HRTEM images of $BiPO_4$ nanocrystals (a, b) before and (c, d) after OA removal.

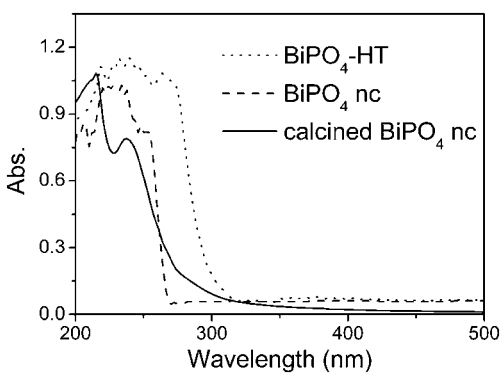

Fig. 3 UV-DRS patterns of $BiPO_4$-HT and $BiPO_4$ nanocrystals ($BiPO_4$ nc) before and after OA removal.

attributed into the transition from O2p states to Bi 6p states as we reported before,[25] and the latter one may be assigned to 6-coordinated bismuth species in the lattice.[36]

3.2 Size control and formation mechanism

The synthesis of well dispersed $BiPO_4$ nanocrystals provides the platform for the formation of primary $BiPO_4$ nanocrystals with tunable sizes. Through tuning the size by varying the synthetic conditions, various functional materials may be obtained, while the reaction process will be well understood as well. In general, the diameters of the synthesised nanocrystals are influenced by reaction time, the concentration of the coordinative ligand and the precipitator. Actually, in our system, if the amount of OA and BEHP is kept constant in the starting mixture, the diameters of as-prepared $BiPO_4$ nanocrystals change slightly, but the shape is changed into rods covered by OA as the amount of Bi^{3+} increases from 0.5 to 5 mmol (Fig. 4a). On the other hand, when the amount of OA is increased from 38 to 60 ml (Fig. 4b), the size of as-prepared $BiPO_4$ nanocrystals particles showed only a small decrease to ~8.3 nm with other conditions held the same. Moreover, when the amount of BEHP is increased from 2 ml to 4 ml (Fig. 4c), the diameter of as-prepared $BiPO_4$ nanocrystals shows a minor increase to 12.5 nm. When the reaction time increases to 3 h (Fig. 4d), the product $BiPO_4$ nanocrystals possess an average of 12.0 nm but a wide particle size distribution, due to defocusing of the growth process.[37] In that case, if the monomer concentration drops below a critical threshold, small nanocrystals are depleted as larger ones grow and the distribution broadens, or defocuses.[37] Therefore, it is very difficult to control the particle size from several to several hundred nanometres by simply changing the sole source or reaction time. These results demonstrate that many other methods should be employed to precisely control the size of $BiPO_4$ nanocrystals.

In this work, a bisolvent synthetic method was introduced to continuously control the size of $BiPO_4$ nanocrystals. It was also reported to succeed in controlling the Fe_3O_4 nanocrystals from 10 to 200 nm by Yu *et al.*[38] During the formation of the $BiPO_4$ nanocrystals, BEHP plays roles as a phosphate source, while OA is served as capping reagent. Not surprisingly, the size of the $BiPO_4$ nanocrystals can be obviously changed by only varying the OA/BEHP ratio. Herein, control experiments using parameters for synthesis of 9 nm $BiPO_4$ nanocrystals were performed by changing the OA/BEHP ratio. Fig. 5a–d show the TEM images of as-prepared $BiPO_4$ nanocrystals, the size of the $BiPO_4$ nanocrystals significantly increased with the amount of BEHP increased. The diameter of the as prepared $BiPO_4$ nanocrystals ranges from 9 to 25, 50, 100, and 250 nm when the OA/BEHP ratio (v/v) changes from 38/2 to 30/10, 25/15, 20/20, and 10/30. The phase purity of $BiPO_4$ nanocrystals obtained is also examined by XRD (Fig. S4, ESI†). All the samples can be indexed as a monoclinic $BiPO_4$ structure. The average crystal size of the primary nanocrystals in the $BiPO_4$ nanocrystals are increased from 8.2 to 17.5, 40.3, 90.1, and >100 nm, respectively, calculated by Scherrer equation from data according to (−111) of Fig. S4, ESI.†The average grain sizes calculated from the XRD peaks are almost the same as the TEM results, revealing that each primary nanocrystal is a single domain. These results suggest that $BiPO_4$ nanocrystals with continuously controlled sizes can be effectively synthesized *via* a simple one-step high-temperature hydrolysis method.

The diameter of the $BiPO_4$ nanocrystals can be adjusted in a wide range due to the good compatibility of BEHP and OA, which makes it easy to tune the size. During the reaction, BEHP may serve as a precipitator and an emulsifier due to its hydrophilic phosphate headgroup and hydrophobic alkyl tail. It is well

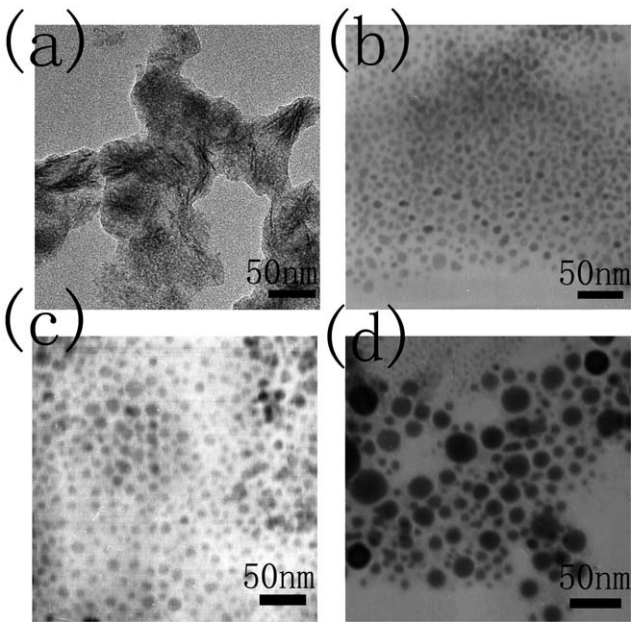

Fig. 4 TEM images of well dispersed $BiPO_4$ nanocrystals obtained at different hydrolysis conditions: (a) 5 mmol $Bi(NO_3)_3$, (b) 60 ml oil, (c) 4 ml BEHP, and (d) at 190 °C for 3 h, each one with other experimental parameters kept constant.

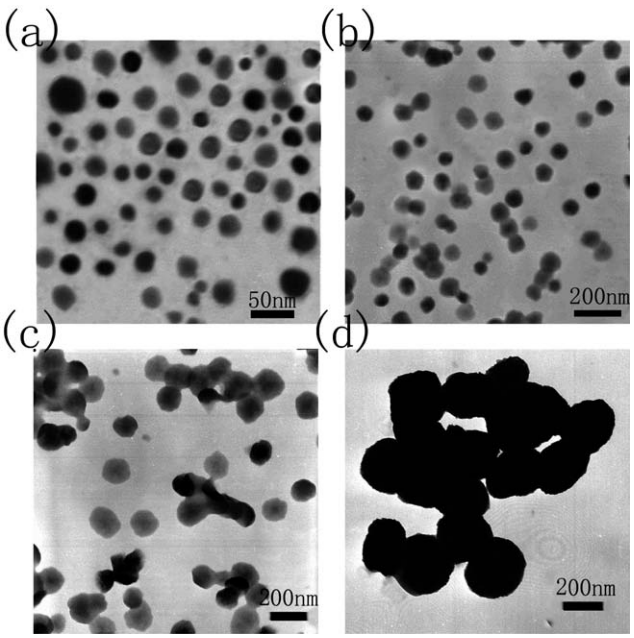

Fig. 5 TEM images of well dispersed $BiPO_4$ nanocrystals obtained at different OA/BEHP ratio (v/v): (a) 30/10, (b) 25/15, (c) 20/20, and (d) 10/30.

known that the phosphate headgroup of phosphate esters can bind metallic cations. This type of interaction is particularly strong in the case of trivalent metal ions like lanthanide and actinide cations.[39,40] In our experiment, BEHP can react firstly with Bi^{3+} to form a complex precipitation, which can subsequently be solvated in OA due to the emulsification of BEHP. Instead of BEHP, when the phosphate source was changed into other inorganic salts like $(NH4)_2HPO_4$ or Na_3PO_4 no transparent solution obtained even after three days stirring, which indirectly implies the coordination effect between Bi^{3+} and BEHP. At the same time, Bi^{3+} will hydrolyze to produce HNO_3 in the solution. This acid solution will accelerate BEHP to hydrolyze producing 2-ethyl-1-hexanol which can be detected with mass spectrometer (Fig. S5, ESI†). As reaction temperature (190 °C) is higher than the boiling point of 2-ethyl-1-hexanol (b.p. 185 °C), the 2-ethyl-1-hexanol is evaporated, which makes the hydrolysis continue to produce $BiPO_4$ nanocrystals.

The role of BEHP is also demonstrated when the reaction is carried out without OA (Fig. 6). In this case, we can also obtain monoclinic $BiPO_4$ but with a large size, more than 300 nm. Therefore, BEHP is both a phosphate source and an emulsifier in the reaction. This also indicates that OA, but not BEHP, can confine the size of the particles effectively.

To detail the nucleation and growth process of the $BiPO_4$ nanocrystals, the TEM images of the evolution of the $BiPO_4$ nanocrystals with time were shown in Fig. 7. In the early stage of reaction (less than 10 min, Fig. 7a), no $BiPO_4$ nuclei are formed, but a significant amount of Bi–BEHP complex is formed. Subsequently at about 30 min in the presence of H^+ the complex was transformed into $BiPO_4$ nuclei through hydrolysis (Fig. 7b). Meanwhile, the freshly formed nanocrystals are unstable because they contain high surface energy, and thus they have a great tendency to aggregate rapidly. Furthermore, $BiPO_4$ nuclei evolve into the larger ones covered by OA due to the strong coordination between bismuth (III) ions and carboxylate (Fig. 7c). The OA coated $BiPO_4$ nuclei may react with each other *in situ*, which would help to form the primary $BiPO_4$ nanocrystals in the recrystallization process.[41] Nanocrystals will further absorb other Bi-BEHP and grow larger due to the good compatibility between BEHP and OA (Fig. 7d).

To understand this process deeply, Fig. 8 shows the XRD patterns during the reaction. There is no obvious peak at 10 min, though the TEM image shows a large particle size. This suggests the precipitator at this time is almost all Bi–BEHP complex, as

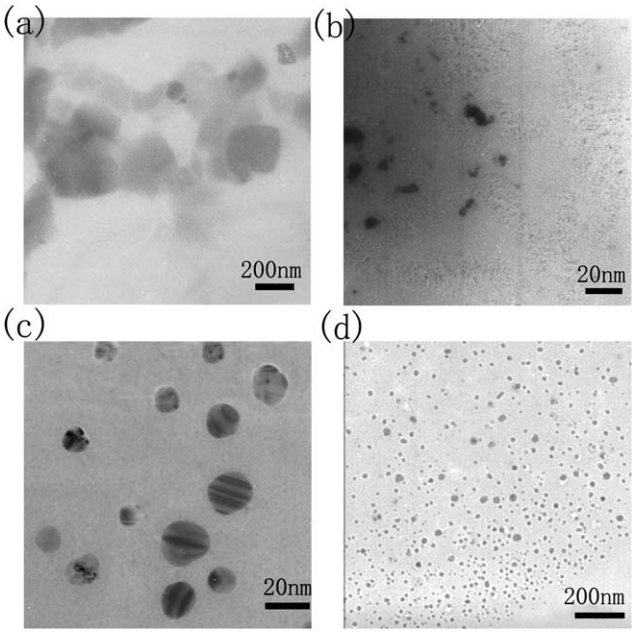

Fig. 7 TEM images of well dispersed $BiPO_4$ nanocrystals obtained at different hydrolysis time: (a) 10 min, (b) 30 min, (c) 1 h, and (d) 2 h.

we mentioned above. From 30 min to 2 h, a clear crystalline process can be seen, according to the increasing of both peak intensity and numbers, which is consistent with the TEM observed results.

According to the above analysis the mechanism for the nanocrystal formation is shown in Fig. 9. The growth of the $BiPO_4$ nanocrystals follows the three-stage growth model in which primary nanocrystals nucleate first in a supersaturated solution and then aggregate into polynanocrystals whereby the original dots can still be distinguished as individual nanocrystals. The main driving force for the aggregation of the nanocrystals' nuclei is generally attributed to the reduction in the high surface energy through attachment among the primary nanoparticles. Finally, these dots then fuse into single crystals though a recrystallization process due to high hydrolysis temperature.[42] During this reaction, the OA/BEHP ratio (v/v) plays a key role in controlling the size of the nanocrystals.

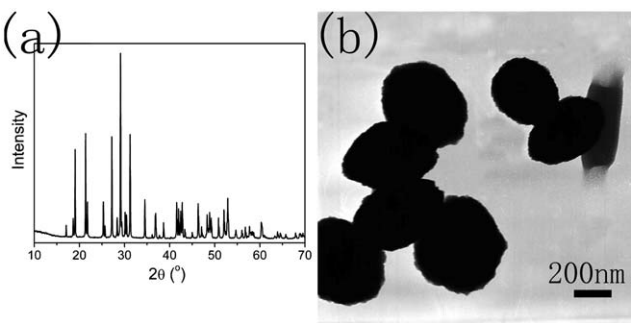

Fig. 6 XRD (a) and TEM (b) of $BIPO_4$ synthesis in BEHP without OA.

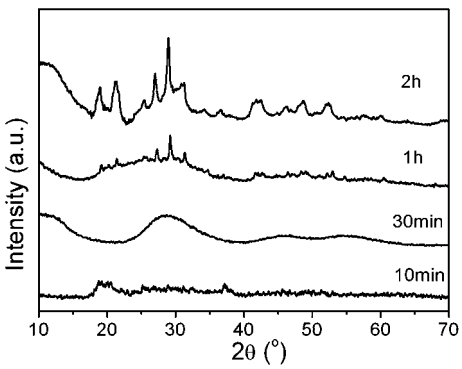

Fig. 8 XRD patterns of well dispersed $BiPO_4$ nanocrystals obtained at different hydrolysis times.

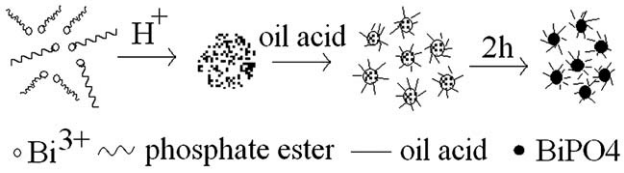

Fig. 9 Proposed formation mechanism of $BiPO_4$ nanocrystals.

3.3 Photocatalytic performance

The MB decomposition catalyzed by $BiPO_4$ nanocrystals with different average crystal size before and after OA removal was investigated, as shown in Fig. 10. Compared to the $BiPO_4$ nanocrystals with OA (Fig. 10A), nanocrystals after OA removal show obviously superior activity (Fig. 10A). In the photocatalytic reaction, the carboxylate group of OA often acts as a hole scavenger, which hinders the production of OH radicals.[43] However, OH radicals are regarded as the main active species for organic pollutant degradation in the $BiPO_4$ system.[25] In addition, nanocrystals with OA absorbed are hydrophobic, and so are also hard to disperse in aqueous solution. Both the above reasons lead to a large activity difference between the $BiPO_4$ nanocrystals before and after OA removal. It is also pointed out that the catalytic activity decreases rapidly with nanocrystals ranging from 9 to 25, 50, 100, and 250 nm. The experimental data demonstrate that MB photodegradation on $BiPO_4$ nanocrystals follows the pseudo-first-order kinetics, as shown in Fig. 11. The order of photocatalytic activity of $BiPO_4$ nanocrystals together with P25 and $BiPO_4$-HT, the activity of which we reported

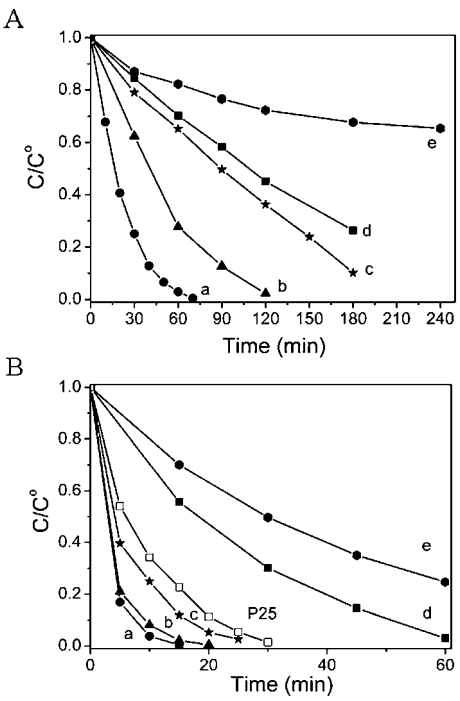

Fig. 10 Photocatalytic degradation curves of MB for $BiPO_4$ nanocrystals with different average grain sizes: (a) 9 nm, (b) 25 nm, (c) 50 nm, (d) 100 nm, and (e) 250 nm, (A) before and (B) after OA removal.

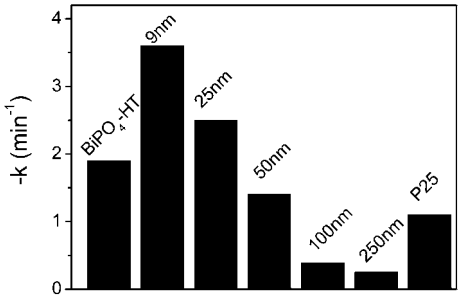

Fig. 11 Photocatalytic activity of MB degradation for $BiPO_4$ nanocrystals after OA removal with different average grain sizes.

before[25] is as follows: k (250 nm) < k (100 nm) < k (P25) < k (50 nm) < k ($BiPO_4$-HT) < k (25 nm) < k (9 nm). The photocatalytic activity of $BiPO_4$ nanocrystals with a diameter of ~9 nm is 3.64 min^{-1}. That is 2.6 times higher than that of P25 (k = 1.01 min^{-1}) and nearly as twice as the bulk $BiPO_4$-HT (k = 1.97 min^{-1}).

There are three main reasons for the good photocatalytic activity of small-sized $BiPO_4$ nanocrystals. First is the large BET surface derived from the small particle size, which is about 75 m^2 g^{-1} for $BiPO_4$ nanocrystals with a diameter of ~9 nm after OA removal. That is 24 times higher than that of $BiPO_4$-HT (3 m^2 g^{-1}), though it is not so large compared to other nanocrystals (commonly larger than 100 m^2 g^{-1}) due to the heavy aggregation. Second is the nanosize effect, which will split the electronic bands of the macro-crystalline material into discrete energy levels followed by band gap broadening. In this experiment, $BiPO_4$ nanocrystals with a diameter of ~9 nm after OA removal have a band gap nearly 0.8 eV higher than the $BiPO_4$-HT. This will be the lower position of the valence band, leading to a higher oxidation potential of holes than that in $BiPO_4$-HT. The third reason is the large surface atom ratio: PO_4^{3-} at the surface will drive the holes to the surface, more of which help to promote the separation between the photogenerated e^-/h^+.[44] The last reason is the small size means short mobility distance to the surface, which will reduce the combination possibility between electrons and holes. In summary, the high BET surface, large band gap, surface effect, and less confinement of electron and hole motions derived from the small size benefits the photocatalytic activity of $BiPO_4$ nanocrystals.

4 Conclusion

Well dispersed $BiPO_4$ nanocrystals with a diameter of ~9 nm have been synthesized by a high-temperature hydrolysis reaction in an OA and BEHP mixture. The diameters of the as prepared $BiPO_4$ nanocrystals have been controlled from 9 nm to 250 nm in relation to the OA/BEHP ratio (v/v). The $BiPO_4$ nanocrystals (~9 nm), after OA removal, show the highest activity for degradation of MB solution of all the prepared $BiPO_4$ nanocrystals, which is also nearly twice the activity of $BiPO_4$, and 2.5 times higher than that of P25 in the UV region. The high BET surface, large band gap, surface effect, and short mobility distance of electron and hole derived from the small size benefit for the high photocatalytic activity. The use of phosphate ester

may be extended to the synthesis of other functional phosphate salts nanocrystals materials.

Acknowledgements

This work was partly supported by the National Natural Science Foundation of China (20925725 and 50972070) and National Basic Research Program of China (2007CB613303).

Notes and references

1 T. Mokari and U. Banin, *Chem. Mater.*, 2003, **15**, 3955–3960.
2 I. Gur, N. A. Fromer, M. L. Geier and A. P. Alivisatos, *Science*, 2005, **310**, 462–465.
3 B. Gregg and A. M. C. Hanna, *J. Appl. Phys.*, 2003, **93**, 3605–3614.
4 N. Tessler, V. Medvedev, M. Kazes, S. Kan and U. Banin, *Science*, 2002, **295**, 1506–1508.
5 A. P. Alivisatos, *J. Phys. Chem.*, 1996, **100**, 13226–13239.
6 M. Bruchez, M. Moronne, P. Gin, S. Weiss and A. P. Alivisatos, *Science*, 1998, **281**, 2013–2016.
7 J. Wang, J. Xu, M. D. Goodman, Y. Chen, M. Cai, J. Shinar and Z. Q. Lin, *J. Mater. Chem.*, 2008, **18**, 3270–3274.
8 M. P. Marder, *Condensed Matter Physics*, John Wiley & Sons, New York, 2000.
9 A. R. West, *Basic Solid State Chemistry*; John Wiley & Sons: New York, 2000.
10 K. Seeger, *Semiconductor Physics*; Springer-Verlag: New York, 1997.
11 X. Chen and S. S. Mao, *Chem. Rev.*, 2007, **107**, 2891–2959.
12 H. Fu, C. Pan, W. Yao and Y. Zhu, *J. Phys. Chem. B*, 2005, **109**, 22432–22439.
13 C. Zhang and Y. Zhu, *Chem. Mater.*, 2005, **17**, 3537–3545.
14 H. Fu, L. Zhang, W. Yao and Y. Zhu, *Appl. Catal., B*, 2006, **66**, 100–110.
15 S. Zhu, T. Xu, H. Fu, J. Zhao and Y. Zhu, *Environ. Sci. Technol.*, 2007, **41**, 6234–6239.
16 H. Fu, S. Zhang, T. Xu, Y. Zhu and J. Chen, *Environ. Sci. Technol.*, 2008, **42**, 2085–2091.
17 L. Zhang, W. Wang, L. Zhou and H. Xu, *Small*, 2007, **3**, 1618–1625.
18 A. Kudo, K. Omori and H. Kato, *J. Am. Chem. Soc.*, 1999, **121**, 11459–11467.
19 T. Saimi, K. Hideki and A. Kudo, *Chem. Mater.*, 2001, **13**, 4624–4628.
20 L. Zhang, D. Chen and X. Jiao, *J. Phys. Chem. B*, 2006, **110**, 2668–2673.
21 T. Xu, C. Zhang, X. Shao, K. Wu and Y. Zhu, *Adv. Funct. Mater.*, 2006, **16**, 1599–1607.
22 M. Shang, W. Wang, S. Sun, L. Zhou and L. Zhang, *J. Phys. Chem. C*, 2008, **112**, 10407–10411.
23 A. Guéguen, P. F. P. Poudeu, C. Li, S. Moses, C. Uher, J. He, V. Dravid, K. M. Paraskevopoulos and M. G. Kanatzidis, *Chem. Mater.*, 2009, **21**, 1683–1694.
24 B. Pejova, I. Grozdanov, D. Nesheva and A. Petrova, *Chem. Mater.*, 2008, **20**, 2551–2565.
25 C. Pan and Y. Zhu, *Environ. Sci. Technol.*, 2010, **44**, 5570–5575.
26 M. Yang, N. K. Shrestha, R. Hahn and P. Schmuki, *Electrochem. Solid-State Lett.*, 2010, **13**, C5–8.
27 Y. F. Lin, H. W. Chang, S. Y. Lu and C. W. Liu, *J. Phys. Chem. C*, 2007, **111**, 18538–18544.
28 Q. Zhang, T. Tojo, W. Tongamp and F. Saito, *Powder Technol.*, 2009, **195**, 40–43.
29 K. V. Terebilenko, I. V. Zatovsky, N. S. Slobodyanik, V. N. Baumer and V. G. Zatovsky, *Inorg. Mater.*, 2007, **43**, 1336–1339.
30 M. Roming and C. Feldmann, *J. Mater. Sci.*, 2009, **44**, 1412–1415.
31 J. P. Ge, W. Chen, L. P. Liu and Y. D. Li, *Chem.–Eur. J.*, 2006, **12**, 6552–6558.
32 H. Mai, Y. Zhang, L. Sun and C. Yan, *Chem. Mater.*, 2007, **19**, 4514–4522.
33 S. Maensiri, C. Masingboon, P. Laokul, W. Jareonboon, V. Promarak, P. L. Anderson and S. Seraphin, *Cryst. Growth Des.*, 2007, **7**, 950–955.
34 T. Ghoshal, S. Kar and S. Chaudhuri, *J. Cryst. Growth*, 2006, **293**, 438–444.
35 G. Zhang, N. Chang, D. Han, A. Zhou and X. Xu, *Mater. Lett.*, 2010, **64**, 2135–2137.
36 G. Qian, D. Ji, G. Lu, R. Zhao, Y. Qi and J. Suo, *J. Catal.*, 2005, **232**, 378–385.
37 X. G. Peng, L. Manna, W. D. Yang, J. Wickham, E. Scher, A. Kadavanich and A. P. Alivisatos, *Nature*, 2000, **404**, 59–61.
38 S. Xuan, Y. J. Wang, J. Yu and K. C. Leung, *Chem. Mater.*, 2009, **21**, 5079–5087.
39 P. G. Barton, *J. Biol. Chem.*, 1968, **243**, 3884–3890.
40 L. Moreau, F. Ziarelli, M. W. Grinstaffc and P. Barthélémy, *Chem. Commun.*, 2006, 1661–1663.
41 C. L. Lin, C. F. Lee and W. Y. Chiu, *J. Colloid Interface Sci.*, 2005, **291**, 411–420.
42 M. A. van Huis, L. T. Kunneman, K. Overgaag, Q. Xu, G. Pandraud, H. W. Zandbergen and D. Vanmaekelbergh, *Nano Lett.*, 2008, **8**, 3959–3963.
43 M. R. Hoffmann, S. T. Martin, W. Choi and D. W. Bahnemann, *Chem. Rev.*, 1995, **95**, 69–96.
44 D. Zhao, C. Chen, Y. Wang, H. Ji, W. Ma, L. Zang and J. Zhao, *J. Phys. Chem. C*, 2008, **112**, 5993–6001.